Journal of Luminescence 132 (2012) 2979–2983

Contents lists available at SciVerse ScienceDirect

Journal of Luminescence

journal homepage: www.elsevier.com/locate/jlumin

Effects of heat treatment and TiO_2 content on the optical properties of Eu^{3+} doped TiO_2–SiO_2 thin films

Oualid Berkani [a,b,*], Khelil Latrous [b], Hicham El Hamzaoui [c], Bruno Capoen [c], Mohamed Bouazaoui [c]

[a] Department of Physics, University Mentouri Constantine, Algeria
[b] Actives Devices and Materials Laboratory, University of Oum El Bouaghi, Algeria
[c] Laboratoire de Physique des Lasers, Atomes et molécules (PhLAM), UMR 8523, Université de Lille 1-Sciences et Technologies, 59655 Villeneuve d'Ascq Cedex, France

ARTICLE INFO

Article history:
Received 7 September 2011
Received in revised form
8 June 2012
Accepted 15 June 2012
Available online 23 June 2012

Keywords:
Sol–gel
TiO_2–SiO_2 thin films
Eu^{3+}
Photoluminescence
Raman spectroscopy

ABSTRACT

The photoluminescence properties of Eu^{3+}-doped TiO_2–SiO_2 thin films were investigated. The films were deposited on silicon substrates by the sol–gel process using the dip-coating method. The molar ratio of TiO_2 content was varied from 25% to 100%, while Europium concentration was fixed to 1%. The obtained films were calcinated at various temperatures ranging from 400 °C to 1300 °C, which allowed determining the optimal conditions for the Eu^{3+} luminescence. Meanwhile, the structure of TiO_2–SiO_2 powders, prepared in the same conditions as the films, was also studied by Raman spectroscopy. It revealed the role of Europium and SiO_2 on the stabilization of the anatase phase and the importance of the silica matrix in the control of titania particle size.

1. Introduction

Recently, great attention has been given to TiO_2–SiO_2 thin films prepared by different methods including sol–gel, radio-frequency magnetron sputtering or different kinds of chemical vapor deposition procedures [1–8]. With a good chemical stability, low thermal expansion coefficient, and high refractive index, TiO_2–SiO_2 binary oxide systems can be used in many applications such as optical waveguides, optical filters, optical sensors, and optoelectronic devices [9–11]. TiO_2–SiO_2 thin films are also suitable to incorporate rare-earth ions [12].

SiO_2–TiO_2 matrices doped with trivalent rare earth ions, such as Eu^{3+} or Er^{3+}, are interesting and promising materials for active planar waveguides due to their advantages such as low process temperature, high homogeneity and possibility of producing materials with controlled refractive indices [13].

The photoluminescent properties of Eu^{3+} ions make it a potential element for use in luminescent materials [14,15]. In addition, it has been found that the properties of TiO_2–SiO_2 binary systems depend strongly on the contents of TiO_2 [16] and annealing temperatures [17].

Zhao et al. reported on the effects of temperature and TiO_2 content on the photoluminescence properties of Eu^{3+}-doped TiO_2–SiO_2 powders. Their results revealed the possible formation of Eu^{3+} aggregates depending on the annealing temperature and on the TiO_2 concentrations [18]. You and Nogami reported on optical properties and local structure of Eu^{3+} ions in sol–gel TiO_2–SiO_2 glasses where they observed an energy transfer from the O–Ti charge-transfer band to the Eu^{3+} ions [19]. At the same time, they found that the emission intensity and the average decay time increase, revealing that the incorporation of TiO_2 can reduce the extent of the Eu^{3+} clusters.

In this work, we report on photoluminescence properties of Eu^{3+}-doped TiO_2–SiO_2 thin films prepared using a sol–gel method and deposited by dip-coating. The Europium concentration was fixed to 1 mol% while the TiO_2 content was varied from 25 mol% to 100 mol%. The effects of the heat-treatment temperature and of the TiO_2 content on the photoluminescence properties of Eu^{3+}-doped TiO_2–SiO_2 thin films were investigated. Moreover, the structure of the resulting powder of TiO_2–SiO_2 sol was also studied by Raman spectroscopy as a function of calcination temperature.

2. Experiments

All chemical products have been purchased from Aldrich and used as-received. The starting solution was obtained by mixing TetraEthylOrthoSilicate (TEOS), ethanol, deionized water, and

* Corresponding author at: Actives Devices and Materials Laboratory, University of Oum El Bouaghi, Oum El Bouaghi 04000, Algeria. Tel.: +213 6 68 04 72 75; fax: +213 32 47 61 55.
E-mail addresses: wberkani@yahoo.fr, w.berkani@univ-oeb.dz (O. Berkani).

0022-2313/$ - see front matter © 2012 Elsevier B.V. All rights reserved.
http://dx.doi.org/10.1016/j.jlumin.2012.06.019

hydrochloric acid as a catalyst. This sol was prehydrolyzed for 1 h at room temperature. The molar ratio of TEOS:HCl:EtOH:H_2O was 1:0.01:37.9:2. An ethanolic solution prepared using titanium isopropoxide and $Eu(NO_3)_3 \cdot 5H_2O$ as precursors was added to the solution containing TEOS. The mixture was left at room temperature under stirring for 1 h. Eu^{3+}-doped TiO_2–SiO_2 films were deposited by dip-coating on silicon substrates using a withdrawal rate of 40 mm/min. Each layer was annealed in air for 15 min at 400 °C prior to the next dip. Finally, the films resulting from 10 coatings were stabilized by a treatment for 30 min in air at 400 °C. To investigate the effect of the calcination temperature on the PL properties, the obtained films have been subsequently heat-treated for 30 min in air at different temperatures comprised between 400 °C and 1300 °C.

The Raman spectra were obtained in a confocal conuration using a triple-grating spectrometer (Jobin-Yvon T64000) and the 514.5 nm line of an Ar^+ laser as the excitation source with a power of 200 mW. All Raman spectra were recorded at room temperature in the wave number range of 50–700 cm^{-1}.

The optical absorption spectra were recorded at room temperature using a Perkin-Elmer Lambda 19 UV–Vis–IR spectrophotometer.

Photoluminescence spectra were recorded at room temperature by exciting the samples with the 351 nm line of an argon laser with a power of 25 mW. The emitted light was imaged onto the slits of a Jobin-Yvon U1000 monochromator and collected using a Hamamatsu R943-02 photomultiplier tube. Moreover, the employed experimental set-up ensures the absolute comparison between the different samples. Indeed, the laser power, the location of the samples, as well as the optical elements (lenses, mirrors, etc.) were kept accurately the same in order to perform an absolute comparison between different spectra.

3. Results and discussion

Fig. 1 shows the transmittance spectra of $50TiO_2$–$50SiO_2$ thin films annealed at different temperatures. These spectra clearly exhibit interference patterns that can be exploited to determine simultaneously the thicknesses and the refractive indices of the layers. The result of this calculation is reported in Fig. 2, which shows the evolution of thickness and refractive index as a function of the heat-treatment temperature for different TiO_2 concentrations. The different values of thickness and refractive index are also summarized in Table 1. It can be seen from Fig. 2 that the film thickness increases with TiO_2 content. For all TiO_2 concentrations in the film, the heat-treatment for 30 min at

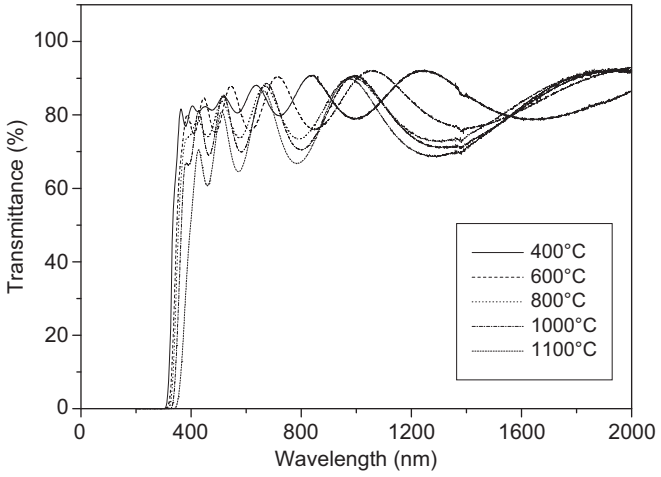

Fig. 1. Optical transmittance spectra of 1% Eu^{3+} $50TiO_2$–$50SiO_2$ thin films.

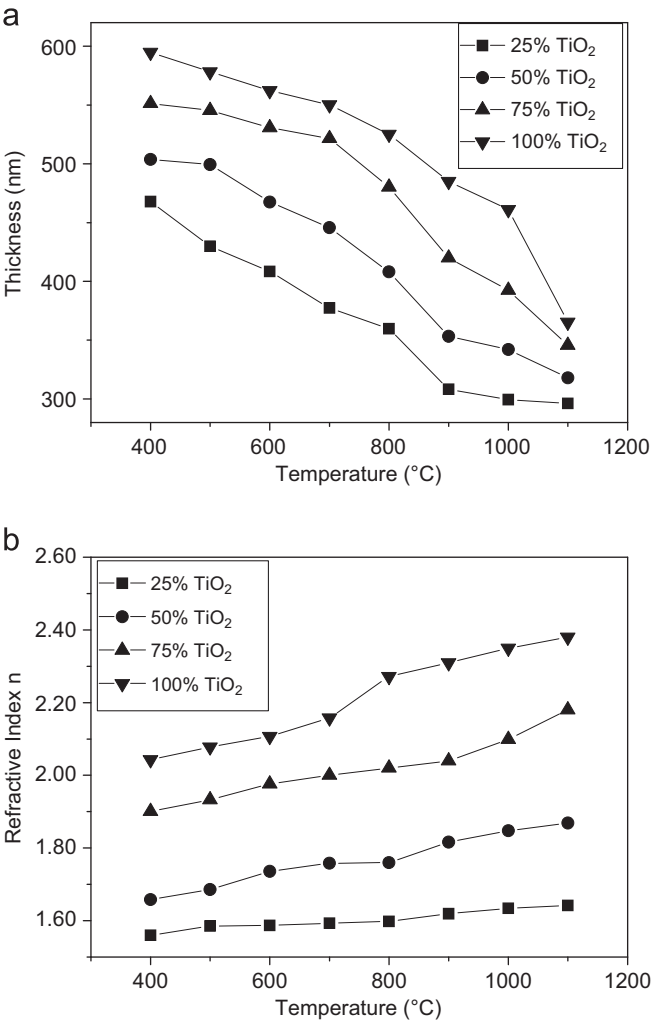

Fig. 2. Thickness (a) and (b) refractive index as a function of the heat-treatment temperature and of TiO_2 content.

Table 1
Thickness (t) and refractive index (n) of $xTiO_2-(100-x)SiO_2$ thin films at different annealing temperatures (T).

T (°C)	$25TiO_2-75SiO_2$		$50TiO_2-75SiO_2$		$75TiO_2-25SiO_2$		100% TiO_2	
	t (nm)	n	t (nm)	n	t (nm)	n	t (nm)	n
400	467.85	1.560	503.67	1.658	551.25	1.901	594.84	2.043
500	429.85	1.585	499.32	1.686	545.37	1.933	578.15	2.078
600	408.50	1.587	467.54	1.736	530.57	1.976	562.23	2.107
700	377.42	1.593	445.79	1.758	521.56	2.000	550.21	2.158
800	359.79	1.598	408.11	1.760	480.33	2.020	525.09	2.272
900	308.21	1.619	353.39	1.816	419.98	2.040	485.06	2.310
1000	299.50	1.634	342.06	1.848	392.39	2.099	460.94	2.350
1100	296.24	1.642	318.00	1.869	345.69	2.180	365.35	2.380

increasing temperatures induces a thickness decrease, together with a refractive index increase. These results could be related to the densification of the films.

Fig. 3 shows the emission spectra under laser excitation at 351 nm of the 1% Eu^{3+}-doped $xTiO_2$–$(100-x)SiO_2$ thin films heated at different temperatures in the range 400–1100 °C. Each PL spectrum, with $x=25$, 50, 75, exhibits five main emission bands at about 579, 594, 613, 653 and 703 nm. These bands correspond to the transitions from the excited $^5D_0$ level to the ^7F_J ($J=0, 1, 2, 3, 4$) levels of Eu^{3+} [20,21]. The peak at 613 nm, arising from the $^5D_0$–$^7F_2$ transition, is responsible for the characteristic

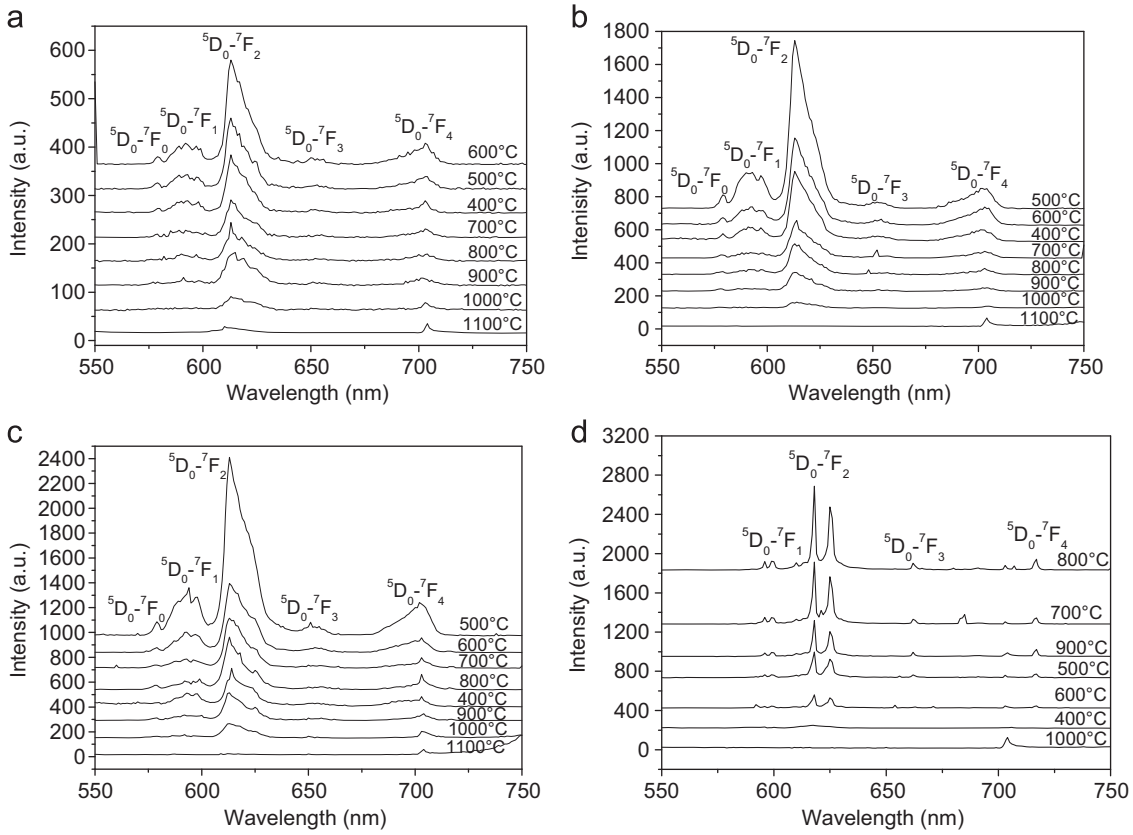

Fig. 3. Emission spectra of the 1% Eu^{3+}-doped $xTiO_2-(100-x)SiO_2$ thin films for various annealing temperatures and for (a) $x=25$, (b) $x=50$, (c) $x=75$ and (d) $x=100$.

red emission of europium ions. It can be seen from Fig. 3 that the intensity of the Eu^{3+} emission increases with the TiO_2 concentration. The maximum was recorded at 600 °C for $x=25$ and at 500 °C for $x=50$ or $x=75$. With increasing annealing temperature, the intensity of the PL begins to increase before decreasing for temperatures higher than 600 °C. This phenomenon is due to the temperature quenching effect [18]. Emission spectra of the 1% Eu^{3+} doped TiO_2 thin films ($x=100\%$) heated at different temperature (400–1000 °C) are shown in Fig. 3(d), revealing sharp emission peaks at 618 nm and 625 nm associated with the $^5D_0$–$^7F_2$ transition of Eu^{3+} under 351 nm excitation. The highest intensities of these peaks were recorded at 800 °C. The weak emission peaks at 596 nm, 662 nm and 717 nm correspond to the 4f–4f intrashell transitions between the first excited state $^5D_0$ and the $^7F_{1,3,4}$ levels. The strong splitting of $^5D_0$–$^7F_2$ transition indicates that Eu^{3+} ions are in two different structural environments, each one differing from the other in the symmetry or in the chemical nature.

Fig. 4 shows the integrated intensity of the $^5D_0$–$^7F_2$ transition as a function of the annealing temperature for each TiO_2 content. The integrated intensity roughly increases with TiO_2 content. However, for pure TiO_2 films, this integrated intensity remains considerably lower. Only for 800 °C, the emission intensity of the sample with concentration $x=100\%$ is higher than the one of other concentrations and it has the same value as for 75% TiO_2. You and Nogami [19] have found that the incorporation of titanium leads to an improvement of the Eu^{3+} surrounding. As a result, more efficient luminescent centers are formed. In their work, they suggest that the titanium ion can reduce the extent of the Eu^{3+} clusters, which are undesirable in most optical materials due to the concentration quenching effects. Therefore, TiO_2 plays an important role in the formation of efficient luminescent centers in the TiO_2–SiO_2 films.

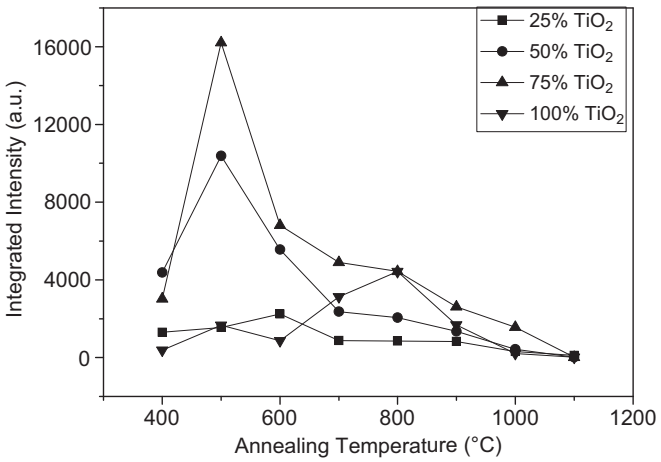

Fig. 4. Integrated intensity of the $^5D_0$–$^7F_2$ transition as a function of annealing temperature for different TiO_2 concentrations.

Fig. 5 shows Raman spectra of 1% Eu^{3+}-doped $xTiO_2$–$(100-x)SiO_2$ powders annealed at different temperatures for 30 min. As it can be seen, anatase phase appears at 400 °C for all samples, while the rutile structure appears at 1000 °C for $x=75$ or 100 and at 1100 °C for $x=25$ or 50. The observed Raman frequencies are listed in Table 2. These spectra attest the phase separation between SiO_2 and TiO_2, a phenomenon also occuring in similar systems such as SiO_2–ZrO_2 [22]. This result shows the influence of europium and of the SiO_2 content on the crystallization of TiO_2. In previous literature [23–25], rutile phase was observed at 800 °C for a pure TiO_2 powder. However in the case of the 1% Eu^{3+}-doped TiO_2 powder, this crystal phase appears at

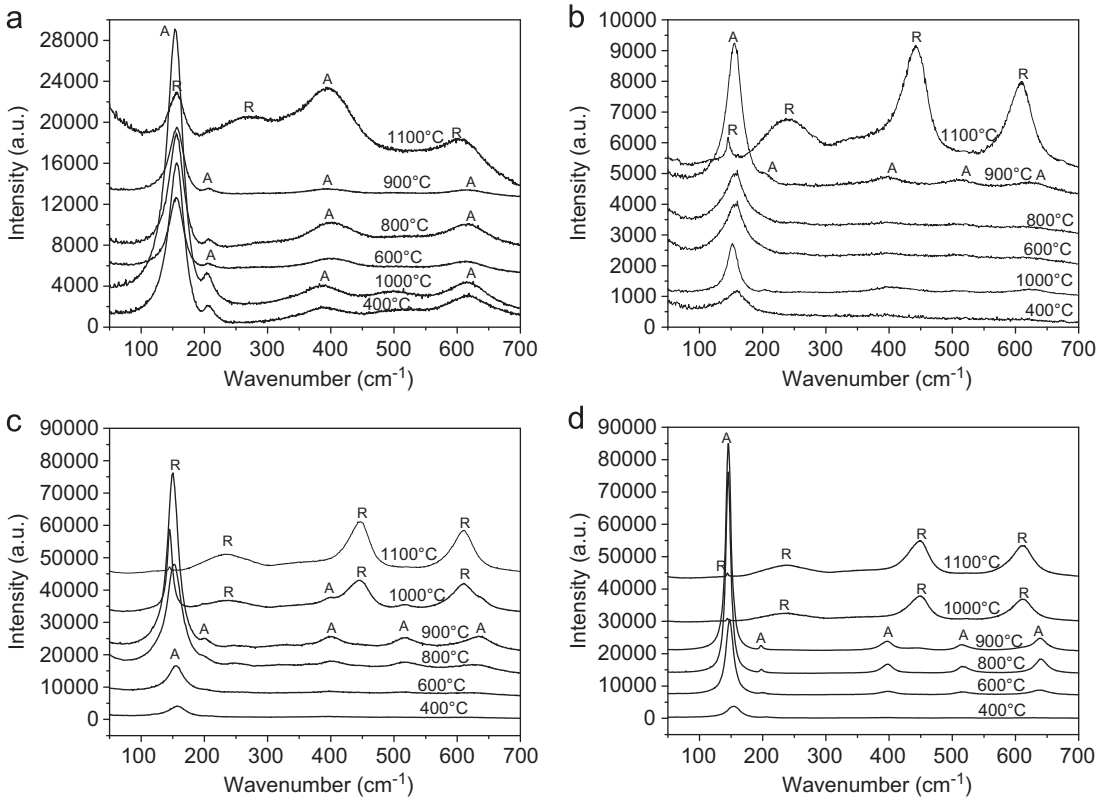

Fig. 5. Raman spectra of 1% Eu^{3+}-doped $xTiO_2-(100-x)SiO_2$ powders annealed at different temperatures for 30 min [(a) $x=25$, (b) $x=50$, (c) $x=75$ and, (d) $x=100$].

Table 2
Observed Raman frequencies (cm^{-1}) and their assignments in $xTiO_2-(100-x)SiO_2$ powders annealed at 800 °C for the anatase phase and 1000–1300 °C for the rutile phase.

	$25TiO_2-75SiO_2$	$50TiO_2-50SiO_2$	$75TiO_2-25SiO_2$	100% TiO_2	Assignement
Anatase					
ν_1	156	155	152	145	E_g
ν_2	207	203	203	197	E_g
ν_3	401	397	399	398	B_{1g}
ν_4	517	501	519	515	A_{1g}
ν_5	517	501	519	515	B_{1g}
ν_6	619	630	629	640	E_g
Rutile					
	145	145	144	144	B_{1g}
	256	237	238	239	Multi-phonon process
	428	442	445	448	E_g
	607	610	611	612	A_{1g}

1000 °C only. This result demonstrates the role of europium ions in the stabilization of the anatase phase. Furthermore, when the SiO_2 content becomes higher than 50%, the rutile phase begins to be observed at 1100 °C only. Therefore, the presence of SiO_2 also plays an important role in the stabilization of the anatase structure of titanium dioxide. Raman spectra can also be used to evaluate the crystallite size. Indeed, a phonon confinement model [26] expresses the relation between the size of TiO_2 anatase nanocrystals and the full-width at half-maximum of the Eg_1 Raman mode. The use of this model clearly shows that the crystallite size does not change upon heat-treatment at a temperature up to 900 °C for 25% SiO_2 and even up to 1000 °C for 75% SiO_2 (Fig. 6). Moreover, Fig. 6 shows that the mean crystallite size remains around 2.5 nm for the highest SiO_2 content ($x \leq 50\%$) while it increases from 2.5 to 15 nm for the samples 25% SiO_2–75% TiO_2 and 100% TiO_2. Such a result demonstrates that SiO_2 matrix impedes the titania crystal growth and can be used to efficiently control the nanocrystal dispersion, as long as TiO_2 remains as a minor part of the whole.

4. Conclusion

Eu^{3+}-doped TiO_2–SiO_2 thin films have been prepared by the sol–gel method. The presence of SiO_2 was found to be important for the stabilization of the anatase form of titanium dioxide and for the particle size control. The heat-treatment of the films leads to a thickness decrease, together with a refractive index increase, at a rate depending on the Ti concentration and on the temperature. The emission spectra of the 1% Eu^{3+}-doped TiO_2–SiO_2 thin films show that the intensity of the Eu^{3+} emission increases with TiO_2 concentration. TiO_2 plays a crucial role in the formation of efficient luminescent centers in the TiO_2–SiO_2 films. Optimal annealing temperature and TiO_2 concentration have been found

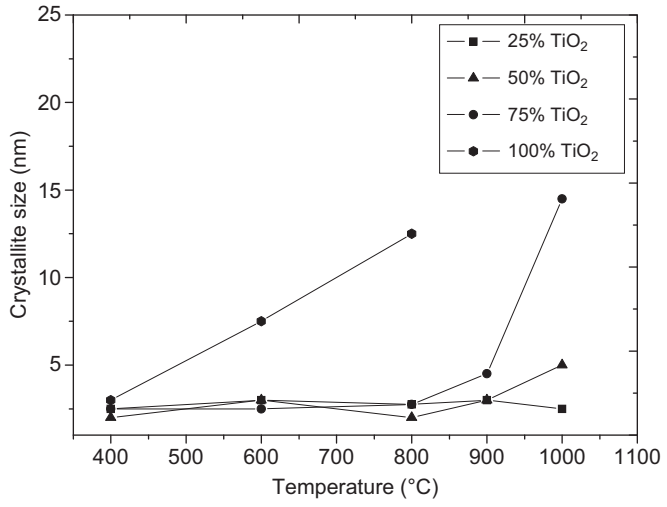

Fig. 6. TiO_2 anatase crystallite size, as a function of the heat-treatment temperature and of TiO_2 content, determined using the FWHM of $E_{g(1)}$ Raman mode and the phonon confinement model [26].

for the europium luminescence intensity. This optimum cannot be ascribed to a particle size, but rather to a better connection between ions and nanocrystals.

Acknowledgments

This work has been realized inside the Centre d'Etudes et de Recherches Lasers et Applications (CERLA), and supported by the Ministère Chargé de la Recherche, the Région Nord/Pas de Calais and the Fonds Européens de Développement Economique des Régions.

References

[1] C.H. Kwon, J.H. Kim, I.S. Jung, H. Shin, K.H. Yoon, Ceram. Inter. 29 (2003) 851.
[2] Y.Y. Liu, L.Q. Qian, C. Guo, X. Jia, J.W. Wang, W.H. Tang, J. Alloys Compd. 479 (2009) 532.
[3] A. Hodroj, H. Roussel, A. Crisci, F. Robaut, U. Gottlieb, J.L. Deschanvres, Appl. Surf. Sci. 253 (2006) 363.
[4] C.F. Song, M.K. Lu, P. Yang, D. Xu, D.R. Yuan, Thin Solid Films 413 (2002) 155.
[5] A. Alvarez-Herrero, G. Ramos, F. del Monte, E. Bernabeu, D. Levy, Thin Solid Films 455 (2004) 356.
[6] M. Wang, B. Gong, X. Yao, Y. Wang, R.N. Lamb, Thin Solid Films 515 (2006) 2055.
[7] C. Battaglin, F. Caccavale, A. Menelle, M. Montecchi, E. Nichelatti, F. Nicoletti, P. Polato, Thin Solid Films 351 (1999) 176.
[8] F. Gracia, F. Yubero, J.P. Holgado, J.P. Espinos, A.R. Gonzalez-Elipe, T. Girardeau, Thin Solid Films 500 (2006) 19.
[9] Z. Jiwei, Y. Tao, Z. Liangying, Y. Xi, Ceram. Int. 25 (1999) 667.
[10] A. Łukowiak, R. Dylewicz, S. Patela, W. Stręk, K. Maruszewski, Opt. Mater. 27 (2005) 1501.
[11] C.F. Song, M.K. Li, P. Yang, D. Xu, D.R. Yuan, Thin Solid Films 413 (2002) 155.
[12] H.P. You, M. Nogami, J. Phys. Chem. B 108 (2004) 12003.
[13] L.Q. Minh, N.T. Huong, C. Barthou, P. Benalloul, W. Strek, T.K. Anh, Mater. Sci. 20 (2002) 2.
[14] C.W. Jia, E.Q. Xie, J.G. Zhao, Z.W. Sun, A.H. Peng, J. Appl. Phys. 100 (2006) 023529.
[15] R. Kudrawiec, M. Nyk, A. Podhorodecki, J. Misiewicz, W. Strek, M. Wolcyrz, Appl. Phys. Lett. 88 (2006) 061916.
[16] J.C. Castañeda-Contreras, M.A.M. Nava, O.B. Garcia, R.A.R. Rojas, M.V. Felix, Opt. Mater. 29 (2006) 38.
[17] I.Z. Zareba-Grodz, R. Pazik, W. Tylus, W. Mielcarek, K. Hermanowicz, W. Strek, K. Maruszewski, Opt. Mater. 29 (2007) 1103.
[18] J. Zhao, H. Duan, Z. Ma, T. Wang, C. Chen, E. Xie, J. Appl. Phys. 104 (2008) 053515.
[19] H. You, M. Nogami, J. Phys. Chem. B 108 (2004) 12003.
[20] K.L. Frindell, M.H. Bartl, A. Popitsch, G.D. Stucky, Angew. Chem.: Int. Ed. 41 (2002) 959.
[21] J. Ovenstone, P.J. Titler, R. Withnall, J. Silver, J. Phys. Chem. B 105 (2001) 7170.
[22] A. Parma, I. Freris, P. Riello, F. Enrichi, D. Cristofori, A. Benedetti, J. Lumin. 130 (2010) 2429.
[23] B. Li, X. Wang, M. Yan, L. Li, Mater. Chem. Phys. 78 (2002) 184.
[24] I.N. Martyanov, K.J. Klabunde, J. Catal. 225 (2004) 408.
[25] S.-C. Hsieh, H. Zhu, T.-Y. Wei, Z.-J. Chung, W.-D. Yang, Y.-H. Ling, J. Eur. Ceram. Soc. 28 (2008) 1177.
[26] K.-R. Zhu, M.-S. Zhang, Q. Chena, Z. Yina, Phys. Lett. A 340 (2005) 220.